Solid State Ionics 28–30 (1988) 1682–1687
North-Holland, Amsterdam

IMPEDANCE SPECTROSCOPY OF SULPHATE SOLID ELECTROLYTES

M. DEKKER, R.A. KALWIJ, J. SCHRAM and J. SCHOONMAN
Laboratory of Inorganic and Physical Chemistry, Delft University of Technology, Julianalaan 136, 2628 BL Delft, The Netherlands

Received 8 September 1987; in revised version 23 October 1987

Sodium sulphate was doped with yttrium sulphate and sodium phosphate, and the ionic conductivity of these compounds was measured using small signal ac response analysis in a wide frequency range (0.1–65000 Hz). From the composition dependence of the bulk conductivity data of these solid solutions the mobilities of the charge carriers contributing to the conduction have been determined. While both sodium ion vacancies and interstitial sodium ions contribute to the conductivity, the sodium ion vacancies constitute the more mobile species. Secondly, the impedance spectra are fitted with an equivalent circuit description. Diffusion limited electrode processes appear to be important in the materials and ambients examined.

1. Introduction

Alkali metal sulphates and MO–MSO_4 thermal decomposition type of electrodes have been studied widely for utilization in potentiometric solid state sensors for sulphur oxides [1–10]. Of the alkali metal sulphates Na_2SO_4 has been studied in detail. This solid electrolyte undergoes phase transformations at 450 K and 575 K. The high-temperature hexagonal form (I) has a modified α-$CaSiO_4$ structure [11], and exhibits suitable solid electrolyte properties [3].

Aliovalent dopants which enhance the sodium vacancy concentration are known to stabilize the high-temperature form [6,7,12,13]. In addition isovalent doping, and ion size effects on the sodium ion conductivity have been reported recently [13], as well as the role of dispersed inert binary oxides [9].

With regard to the defect structure conflicting results have been reported. Usually Frenkel disorder is assumed to prevail with sodium ion vacancies being the more mobile species. Conductivity isotherms for the system Na_2SO_4–$Y_2(SO_4)_3$ lead Saito et al. [7] to the conclusion that sodium interstitials constitute the more mobile species. Leblanc et al. [13] suggest for the system Na_2SO_4–Na_4SiO_4 that sodium excess is compensated by SO_4^{2-} vacancies.

In many studies the defect structure has been studied from either mono-frequency measurements, or impedance spectra recorded in a very limited frequency range [7,8,12,13]. Saito et al. [7] attribute the observed frequency dependence to grain boundary polarization phenomena. In addition, high dopant levels, causing defect–defect interactions also hamper an unambiguous interpretation of the composition dependence of the ionic conductivity of these solid solutions.

In the present study we have used impedance spectroscopy in a wide range of frequencies, and electrical equivalent circuit descriptions for the characterization of the bulk and interface properties of solid solutions Na_2SO_4–$Y_2(SO_4)_3$ and Na_2SO_4–Na_3PO_4.

2. Defect chemistry

Jacob and Rao [3] have shown that the transference number for sodium ions in Na_2SO_4 is unity. Hence, Na_2SO_4 is assumed to exhibit Frenkel disorder, i.e. using Kröger–Vink notation,

$$Na_{Na}^{\times} + V_i^{\times} = Na_i^{\cdot} + V'_{Na}, K_F. \quad (1)$$

Incorporation of $Y_2(SO_4)_3$ enhances the sodium ion vacancy concentration via

0 167-2738/88/$ 03.50

$$Y_2(SO_4)_3 = 2Y_{Na}^{\cdot\cdot} + 4V_{Na}' + 3(SO_4)_{SO_4}^{\times} \quad (2)$$

while incorporation of Na_3PO_4 leads to enhanced interstitial concentrations via

$$Na_3PO_4 = 2Na_{Na}^{\times} + Na_i^{\cdot} + (PO_4)_{SO_4}'. \quad (3)$$

Assuming both intrinsic defects to be mobile the high temperature ionic conductivity σ is given by

$$\sigma = qK_F^{0.5}(\mu_{V_{Na}'} + \mu_{Na_i^{\cdot}}). \quad (4)$$

Here μ denotes mobility, $K_F^{0.5}$ ($= [V_{Na}'] = [Na_i^{\cdot}]$) the intrinsic defect concentration, and q the elementary charge.

3. Experimental aspects

3.1. Materials and preparation

Solid solutions of Na_2SO_4 and $Y_2(SO_4)_3$ were prepared by adding Y_2O_3 to a solution of Na_2SO_4 in H_2SO_4. The powders, which resulted after distilling off the acid, were heated for 6 h at 800°C and grinded. Pellers were made of these powders by applying a hydrostatic pressure of 630 MPa. The pellers were sintered at 800°C for 24 h. Solid solutions of Na_2SO_4 and Na_3PO_4 were prepared by freeze-drying. Sintering occurred at 750°C. Pellets were made as mentioned above.

DTA and X-ray diffraction analyses were carried out to examine the materials on structure, and microprobe analysis was carried out to examine the homogeneity. Finally, Pt was sputtered on both sides of the electrolytes with a sputter coater (Edwards S150B).

3.2. Electrical measurements

ac small signal response measurements were carried out as a function of temperature, using a computer-controlled Solartron 1250 frequency response analyser in the frequency range 0.1–65000 Hz. The amplitude of the sine voltage was 200 mV. Introductory measurements indicated that linearity of the sample was conserved at this value. The pellets were held between two Pt-contacts by spring loading in a metal conductivity cell provided with resistive heating. In all measurements an ambient of air was maintained. A complex non-linear least squares method has been used to fit the measured frequency dispersion of the cell to an equivalent electrical circuit description. An integrated software package was developed, involving coordinated data storage, graphical presentation, and a Marquardt non-linear least squares parameter estimation for complex data.

4. Results and discussion

The structural analyses indicate that solid solutions are formed in all cases. In $Na_2SO_4 \cdot Y_2(SO_4)_3$ with $Y_2(SO_4)_3 > 2$ at%, the hexagonal high temperature phase of Na_2SO_4 is stabilized down to room temperature. However, some endothermal effects are still present below 350°C, according to the DTA curves. These effects cannot be ascribed to a phase transition between two different Na_2SO_4 like structures. The 1 at% $Y_2(SO_4)_3$ shows the usual phase transition in Na_2SO_4 to be shifted to a lower temperature.

All Na_2SO_4–Na_3PO_4 samples exhibit a Na_2SO_4(III) like phase, and a phase transition near 235°C According to X-ray analysis, this phase does not disintegrate slowly into the Na_2SO_4(V) phase, which is an indication that solid solutions are formed [14].

From the temperature dependence of the bulk ionic conductivity of all solid solutions we have constructed conductivity isotherms. The initial linear rise of the isotherms for Na_2SO_4–$Y_2(SO_4)_3$ as depicted in fig. 1a can be ascribed to an increase in sodium ion vacancy concentration. Beyond 3 at% $Y_2(SO_4)_3$ a decrease of the conductivity occurs. Usually this dependence is explained by the formation of defect clusters, e.g. $(Y_{Na}V_{Na})^{\cdot}$. The influence of clusters appears to be bigger at lower temperatures. More research on this matter, however, will be published elsewhere. From the slope of the first part of the curves the mobility of V_{Na}' is calculated as a function of temperature and presented as an Arrhenius plot in fig. 1b.

The conductivity isotherms for Na_2SO_4–Na_3PO_4 (fig. 2a), however, do not show clearly an increase or decrease in conductivity for low amounts of do-

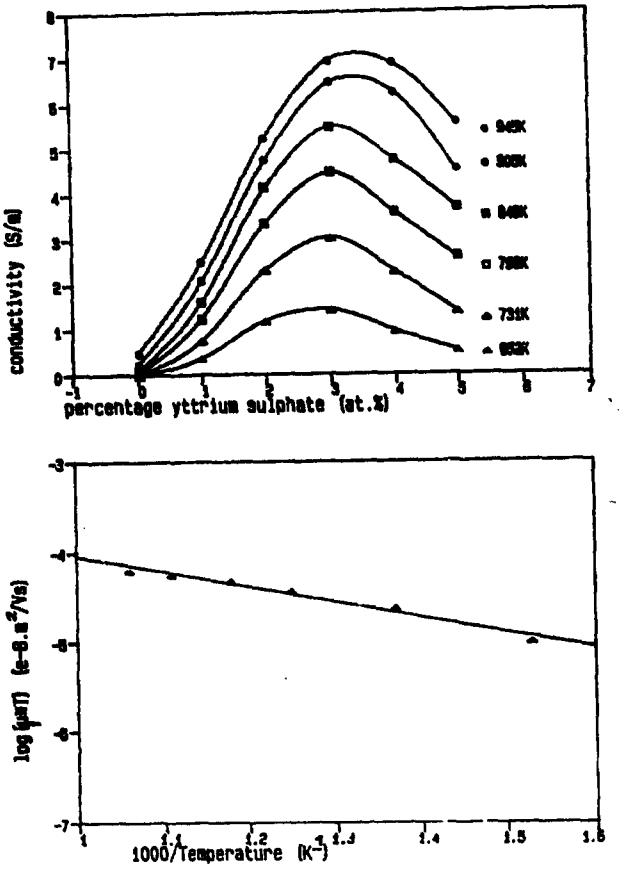

Fig. 1. (a) Bulk conductivity isotherms for Na_2SO_4·x at% $Y_2(SO_4)_3$ (x=0–5 at%). (b) Mobility of sodium ion vacancies in Na_2SO_4·x at% $Y_2(SO_4)_3$, calculated from the slopes of the isotherms between x=0 and x=3 at% in (a).

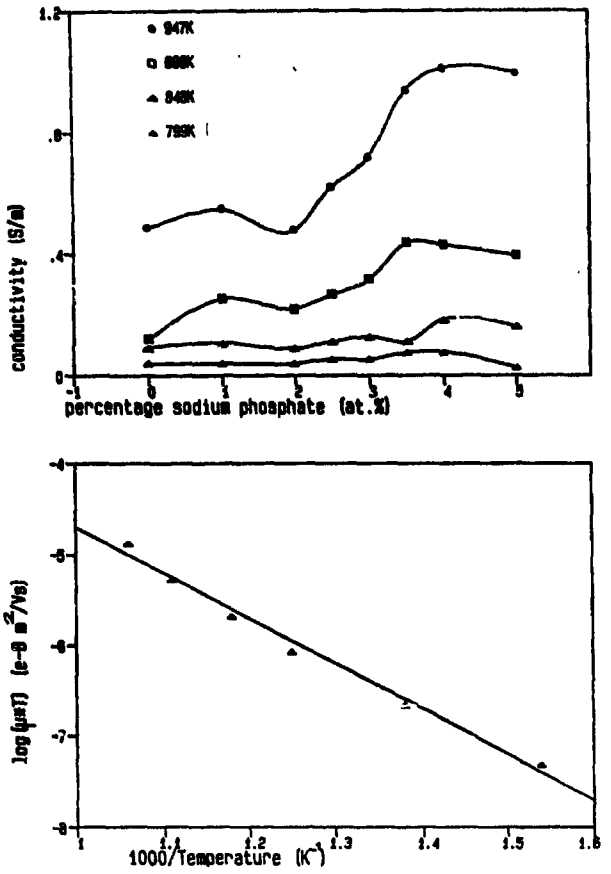

Fig. 2. (a) Bulk conductivity isotherms for Na_2SO_4·x at% Na_3PO_4 (x=0–5 at%). (b) Mobility of interstitial sodium ions in Na_2SO_4·4 at% Na_3PO_4, calculated from the bulk conductivity.

pant (<2.5 at%). As the sodium ion vacancy concentration is lowered by aliovalent anion doping and hence the interstitial sodium ion concentration is increased, these curves can be explained by considering the contribution of both charge carriers giving an area between 0 and 2.5 at% dopant, where both conducting mechanisms compete. For more than 2.5 at% dopant the interstitial ion concentration will be high enough to dominate the conductivity, and an increase in conduction is observed. Beyond 4 at% dopant, defect clustering is the probable cause of the decrease in conductivity.

One can estimate the mobility of $Na_i^{\bullet}$ from the isotherms assuming that the conductivity is dominated by $Na_i^{\bullet}$ completely for 4 at% dopant, and that defect clusters do not form yet at that concentration. The result is given in fig. 2b. By comparing with fig. 1b, it can be seen that, due to the more pronounced dependence on temperature of the interstitial ion mobility, the contribution of $Na_i^{\bullet}$ to the conductivity can no longer be neglected at the higher temperatures when the concentration is sufficiently high. It is also apparent that aliovalent cation doping leads to a negligible contribution of $Na_i^{\bullet}$ to the conductivity at all temperatures, which confirms the straight lines between 0 and 3 at% $Y_2(SO_4)_3$ in fig. 1a.

Following Saito et al. [7], who attributed a frequency dependent conductivity of polycrystalline Na_2SO_4 to grain boundary effects, we have employed the equivalent circuit description as given in fig. 3a to fit the immittance spectra. The circuit is comprised of a bulk resistance R_b and a double layer capacitance C_{dl}, connected in parallel with a constan-

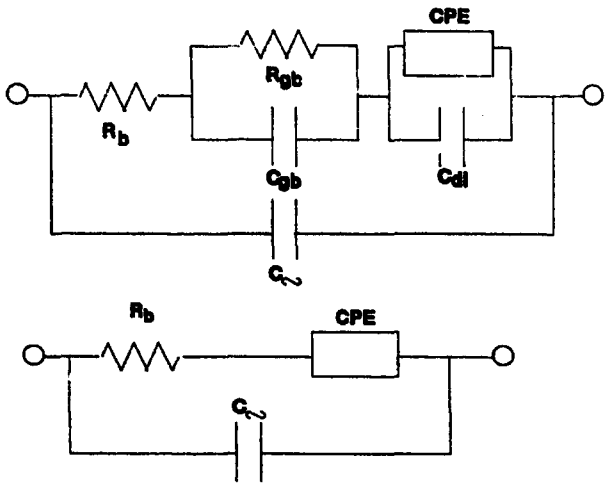

Fig. 3. (a) General equivalent circuit description for ionic conduction in polycrystalline Na_2SO_4. (b) Simplified equivalent circuit description for ionic conduction in Na_2SO_4.

phase element (CPE) Q with impedance $Z_Q = A_Q(i\omega)^{-\alpha}$, representing diffusive or Faradaic electrode effects, while the grain boundary effects are represented by a capacitance C_{gb} and a resistance R_{gb} connected in parallel. Finally, the high frequency geometrical capacitance C_g completes the circuit.

Some preliminary fit calculations revealed a reduced circuit comprising a bulk resistance and a CPE in series to adequately describe the ac response of the impedance of the cell. This reduced circuit is shown in fig. 3b. Above 500°C, the double layer capacitance was separated from the diffusion effect. The CPE Q was replaced then by a Warburg impedance W (with $Z_W = A_W(i\omega)^{-0.5}$), so that the same number of parameters was conserved.

An advantage of this rather simple model description is the limited number of parameters, leading to rapid and unambiguous convergence during the complex nonlinear least squares calculation. Moreover, the parameters appear to be determined with a reasonable accuracy (error $< 7\%$ for the A_Q, and $< 10\%$ for the R_b below 500°C).

Some results obtained with this model are presented in fig. 4(a–c). Especially in the low frequency part of the dispersions an excellent fit was found. The temperature dependence of the constant in the CPE is shown in fig. 5. At temperatures below 500°C, the value A_Q of the element Q is used, while above 500°C the value of the constant A_W of the Warburg impedance is used.

Below about 400°C, a clear Arrhenius-like dependence is found. The slope at low temperatures is found in a region where the $\alpha_Q = 0.55$. The activation enthalpy is 0.30 eV. Above 250°C, the slope of the temperature dependence is increasing, giving an enthalpy of 0.55 eV. In this region an α_Q is found of about 0.75, indicating that double layer effects play an important role in this region. From 500°C onwards, however, the temperature dependence is disturbed, indicating the simple equivalent circuit description to fail, although replacement of the CPE by a Warburg element, and a double layer capacitance yielded an improvement of the fit at those temperatures as compared to the use of a CPE element. Other effects like charge transfer phenomena, as a result of oxygen starting to participate in an electrode reaction may be the cause of this anomalous behaviour. This is presently under study.

The geometrical capacitance could be neglected at temperatures above 250°C, because its determination then required frequencies well above 65 kHz. The value at low temperatures is about 40 pF and is approximately independent of temperature.

Above 500°C, a double layer capacitance was connected in parallel with the Warburg element, as was mentioned before. The value decreased gradually from 434 μF at 502°C down to about 25 μF at 693°C.

Due to the predominant electrode effects in the experimental dispersion, the determination of parameters for grain boundary effects, if present at all, lead to ambiguous results and statistically insignificant values were found. In the high frequency part, however, a qualitative improvement of the fit can be seen especially at low temperatures (fig. 4d). By varying the size parameters of the cell, bulk effects can be made predominant above electrode effects, and an unambiguous determination of the grain boundary parameters can then be made. Our current research is directed towards resolving this matter.

5. Concluding remarks

In Na_2SO_4 both sodium ion vacancies, and sodium interstitials are mobile. The sodium ion vacancy constitutes the more mobile species. The

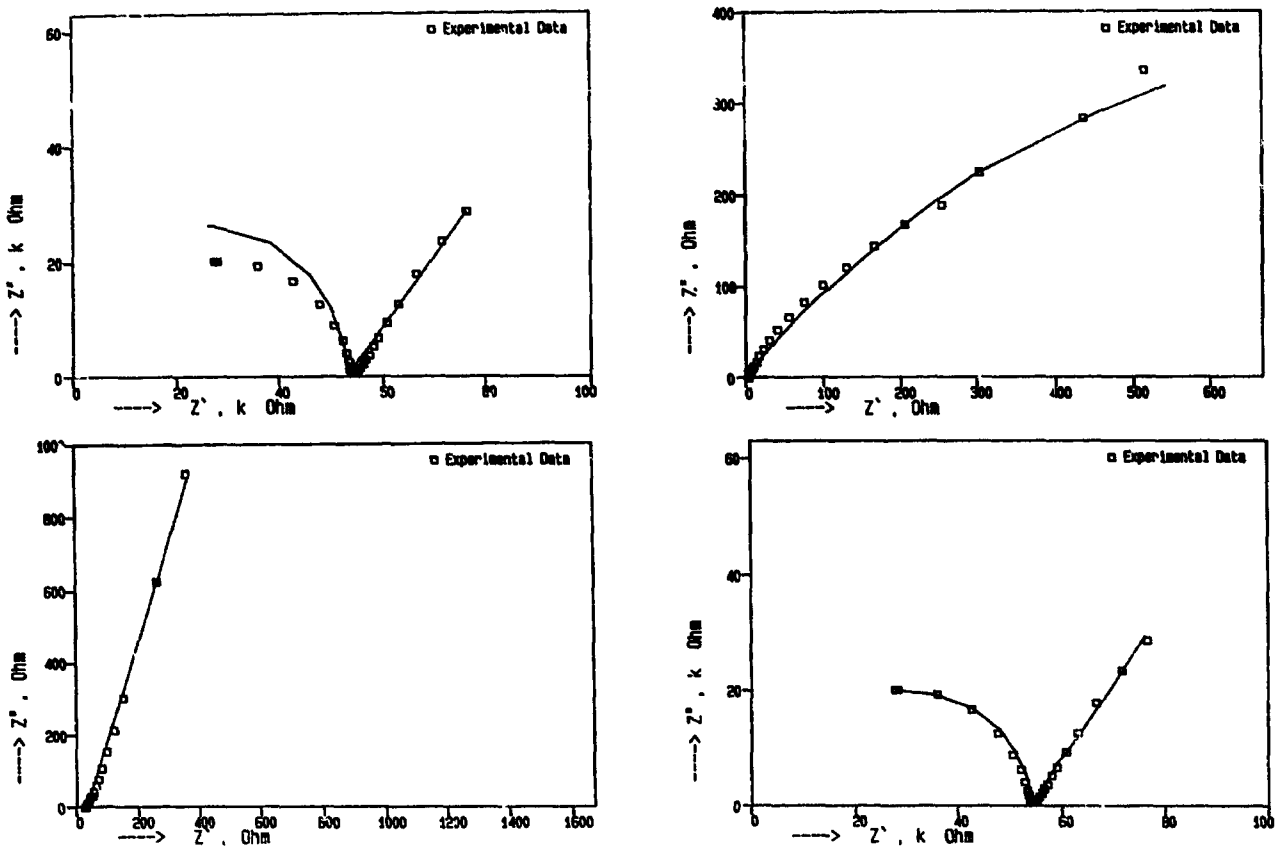

Fig. 4. (a) Experimental spectrum and NLLS-fit, $T=150°C$; (b) Experimental spectrum and NLLS-fit, $T=379°C$: (c) Experimental spectrum and NLLS-fit, $T=672°C$; (d) NLLS-fit with inclusion of grain boundary effects, $T=150°C$.

conductivity data and present analyses lead to a consistent defect description in which SO_4^{2-} vacancies need not be included. The intrinsic ionic conductivity in Na_2SO_4 is determined by two charge carriers, V'_{Na} and $Na_i^{\cdot}$.

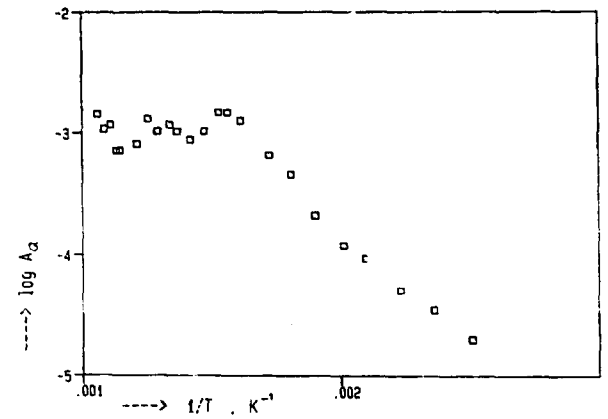

Fig. 5. Temperature dependence of A_Q in the simplified circuit description. Above 500°C, A_W is presented.

The frequency dispersions could be analysed by fitting the curves with a NLLS–Marquardt method. A simple circuit comprising a bulk resistance, a CPE and a geometrical capacitance, suffices for a reasonable description in the temperature range from 100 to 500°C. Contrary to the attribution to grain boundary polarisation effects by Saito et al. [7] on the basis of a limited number of measuring frequencies, the present analysis of immittance spectra reveal electrode interface phenomena to dominate the frequency dispersion. Although their nature has yet to be established, the analysis strengthens the necessity to study the electrical properties of these solid solutions in a wide range of frequencies.

Acknowledgement

The authors are indebted to Dr. Ir. G. Hakvoort for the DTA analysis, to J.F. van Lent for X-ray diffraction, and to D.P. Nelemans for microprobe analyses.

References

[1] M. Gauthier and A. Chamberland, J. Electrochem. Soc. 124 (1977) 1579.
[2] M. Gauthier, A. Chamberland, A. Belanger and M. Poirier, J. Electrochem. Soc. 124 (1977) 1584.
[3] K.T. Jacob and D.B. Rao, J. Electrochem. Soc. 126 (1979) 1842.
[4] M. Gauthier, R. Bellemare and A. Belanger, J. Electrochem. Soc. 128 (1981) 371.
[5] W.L. Worrell and Q.G. Liu, in: Proc. Intern. Meeting on Chemical Sensors, Fukuoka, Japan, 1983, eds. T. Seiyama, K. Fueki, J. Shiokawa and J. Suzuki (Kodansha LED, Tokyo/Elsevier, Amsterdam, 1983) p. 332.
[6] N. Imanaka, G. Adachi and J. Shiokawa in: Proc. Intern. Meeting on Chemical Sensors, Fukuoka, Japan, 1983, eds. T. Seiyama, K. Fueki, J. Shiokawa and J. Suzuki (Kodansha LED, Tokyo/Elsevier, Amsterdam, 1983) p. 348.
[7] Y. Saito, T. Maruyama and K. Kobayashi, Solid State Ionics 14 (1984) 265.
[8] Y. Saito, T. Maruyama, Y. Matsumoto, K. Kobayashi and Y. Yano, Solid State Ionics 14 (1984) 273.
[9] N. Imanaka, Y. Yamaguchi, G. Adachi and J. Shiokawa, J. Electrochem. Soc. 132 (1985) 2519.
[10] Q.G. Liu, W.L. Worrell, Solid State Ionics 18/19 (1986) 524.
[11] W. Eysel and Th. Hahn, Z. Kristallogr. 131 (1970) 322.
[12] K. Shahi and G. Prakash, Solid State Ionics 18 (1986) 544.
[13] M. Leblanc, U.M. Gundusharma and E.A. Secco, Solid State Ionics 20 (1986) 61.
[14] D.M. Wiench and M. Jansen, Z. Anorg. Allg. Chem. 486 (1982) 57.